Experimental proof-of-concept of bubble column evaporative cooling for PEMFC heavy-duty vehicle thermal management

Citation for the original published paper (version of record):
Bosser, C., Sedarsky, D. (2026). Experimental proof-of-concept of bubble column evaporative cooling for PEMFC heavy-duty vehicle
thermal management. Case Studies in Thermal Engineering, 80.
http://dx.doi.org/10.1016/j.csite.2026.107876

Case Studies in Thermal Engineering 80 (2026) 107876

Contents lists available at ScienceDirect

Case Studies in Thermal Engineering

journal homepage: www.elsevier.com/locate/csite

Experimental proof-of-concept of bubble column evaporative cooling for PEMFC heavy-duty vehicle thermal management

Christian Boßer [a,b,*], David Sedarsky [a,b]

[a] Chalmers University of Technology, TechForH2 Excellence Center, Hörsalsvägen 7A, 412 96, Gothenburg, Sweden
[b] Department of Mechanics and Maritime Sciences, Chalmers University of Technology, Hörsalsvägen 7A, 412 96, Gothenburg, Sweden

HIGHLIGHTS

- Novel bubble column evaporative cooling concept for fuel cell thermal management.
- Complementing established radiator cooling system in heavy-duty fuel cell trucks.
- Utilizing pressurized fuel cell exhaust air flow to evaporate product water.
- Validation for up to 1.22 m/s superficial gas velocity in proof-of-concept shown.
- Additional 153 kW cooling for 23 min leads to >40% increase over radiator alone.

GRAPHICAL ABSTRACT

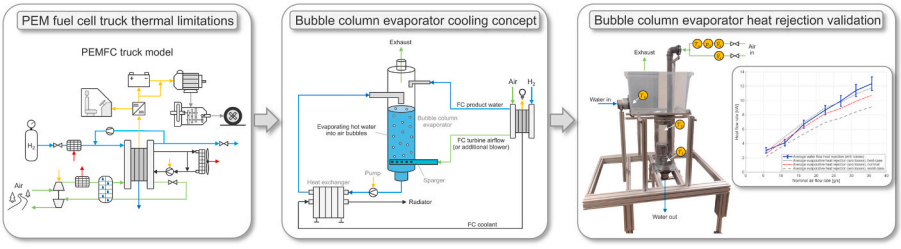

ARTICLE INFO

Keywords:
PEMFC
Heavy-duty
Thermal management
Evaporative cooling
Bubble column
Latent heat
Hydrogen

ABSTRACT

Challenging heat rejection caused by small temperature differences between ambient air and low-temperature proton exchange membrane fuel cells (PEMFC) lead to significantly increased radiator dimension and fan power requirements, increasing the need for alternative cooling solutions. To overcome these limitations, the high latent heat of water that is produced in the hydrogen PEMFC can be utilized to enhance the overall system heat rejection.

A novel bubble column evaporator concept for fuel cell (FC) thermal management has been developed. High heat and mass transfer rates make bubble columns a promising alternative to evaporate the product water. It consists of a semi-closed loop in which heat is transferred from the FC coolant to a secondary water circuit that is evaporatively cooled by injecting the FC exhaust air into a bubble column. This solution utilizes only air and water for cooling, provides additional heat storage, improves with increasing altitude and does not increase the vehicle's drag.

We present the novel counterflow bubble column evaporator concept together with proof-of-concept measurements to demonstrate its viability by validating theoretically predicted heat rejection rates. Higher superficial gas velocities than previously reported have been investigated to reduce system size, reaching up to 1.22 m/s. Based on the presented measurements and a

* Corresponding author. Hörsalsvägen 7A, 412 96, Gothenburg, Sweden.
E-mail address: bosserc@chalmers.se (C. Boßer).

https://doi.org/10.1016/j.csite.2026.107876
Received 12 November 2025; Received in revised form 12 February 2026; Accepted 27 February 2026
Available online 4 March 2026

verified heavy-duty PEMFC truck model, this approach could complement the conventional truck cooling system with 153 kW additional heat rejection for 23 min with 50 kg of water storage. At 20 °C, this corresponds to an increase of over 40% compared to the conventional cooling system alone.

Nomenclature

Abbreviations	
BC	**B**ubble **c**olumn
BCE	**B**ubble **c**olumn **e**vaporator
BR	**B**raking **r**esistor
FC	**F**uel **c**ell
FCS	**F**uel **c**ell **s**ystem
FCEV	**F**uel **c**ell **e**lectric **v**ehicle
FS	**F**ull **s**cale
HD	**H**eavy **d**uty
MFC	**M**ass **f**low **c**ontroller
PEMFC	**P**roton **e**xchange **m**embrane **f**uel **c**ell
RD	**R**ea**d** value
SGV	**S**uperficial **g**as **v**elocity
SRSS	**S**quare-**r**oot of the **s**um of **s**quares
Symbols	
A	Area
c_p	Constant pressure specific heat capacity
d	Diameter
h	Height
Δh_v	Enthalpy of vaporization
$\dot{m}$	Mass flow rate
p	Pressure
$\dot{Q}$	Heat flow rate
T	Temperature
ΔT	Temperature difference
t	Time
$\dot{V}$	Volume flow rate
v	Velocity
Greek symbols	
σ	Standard deviation
φ	Relative humidity
ω	Absolute humidity ratio
Subscripts	
$0, 1, 2, 3, 4$	Measurement/time points
a	Air
dry	Dry (air)
amb	Ambient
avg	Average
$column$	Bubble column
e	Exhaust
$evap$	Evaporation
FC	Fuel cell
g	Gas
i	Inlet conditions
l	Liquid
lat	Latent (heat)
max	Maximum value
min	Minimum value
o	Outlet conditions
sat	Saturation (pressure)
$sens$	Sensible (heat)
sf	Superficial (velocity)
v	Vapor
t	Total
w	Water

1. Introduction

The high latent heat of water can be an effective tool for heat dissipation, especially given its abundance, absence of toxicity, and

ubiquitous role in the environment. One needs to look no further than one's own body to see important levels of latent heat exchange. Sweating leads to water evaporation on the human skin and inhaled air is evaporatively cooled and conditioned in the nasal cavity, supplementing the heat regulation in the human body [1,2]. For fuel cell systems (FCS) which react hydrogen to produce water, electricity, and substantial waste heat, it is also possible to supplement cooling capacity by utilizing the latent heat of water to significant advantage.

Due to their high efficiency and power density, proton exchange membrane fuel cells (PEMFCs) are a promising technology in the challenge to decarbonize heavy-duty (HD) long-haul transport. Despite many advantages, challenges regarding lifetime, cost and thermal management remain [3–6]. One critical challenge is the thermal management of low-temperature PEMFCs because accurate control of its operating temperature is required to achieve high fuel cell (FC) efficiencies and reduced degradation effects, also directly linked to the FC water management. The low operating temperature, typically ranging from 60 to 80 °C or up to 90 °C for short periods, results in challenging cooling of the FC caused by the small temperature difference between the PEMFC and ambient temperature. The required radiator dimensions and fan power to overcome challenging operating conditions like hill climbs therefore significantly increase, making alternative cooling solutions desirable [4–8].

Comprehensive overviews of different PEMFC thermal management methods and enhancements have been presented, for example, in Refs. [4], [9–11]. One of the most promising approaches to enhance the heat transfer in HD FC vehicles which require higher power than passenger cars and often operate at full load, is to utilize the high latent heat of a phase change to reject or temporarily store heat. Latent heat can be utilized either by evaporation or boiling processes or materials that change phase between solid and liquid. To achieve boiling at low-temperature PEMFCs operating ranges, typically refrigerants are required, either flowing through the FC cooling channels or in an external loop, see e.g. Refs. [12–15]. Phase change materials that melt and solidify at these temperatures can be directly built into or around the FC or be part of the external liquid cooling loop [16,17]. Utilizing the FC product water as a non-toxic or flammable working fluid for evaporative cooling has been investigated through different methods in previous studies. The product water has been directly injected into the cathode air stream or cell structure, showing high heat rejection rates but challenges like balancing FC humidification and flooding can arise and structural changes to the FC itself might be required, see e.g. Refs. [4,9,11,18]. Since HD FC trucks might also need to dissipate surplus power from regenerative braking as additional heat during downhill driving to prevent the friction brakes from overheating [19], the heat rejection improvements should not just consider the FC heat removal. By spraying the collected product water onto the radiator, high heat rejection rates have been achieved although challenges like water spillage, blocked air flow channels, low water utilization rates or fouling especially in off-road applications have been identified, see e.g. Refs. [20–23]. Critical aspects of alternative or supplementary thermal management solutions are cost, weight, volume, complexity and auxiliary power consumption [4,9].

In this work we present a novel bubble column cooling concept suitable for heavy-duty truck fuel cell systems together with test data from a proof-of-concept test bench. The high evaporative heat and mass transfer achievable in bubble columns (BCs) reported in literature has led to the development of the bubble column evaporator (BCE) cooling concept that we presented in Ref. [24]. Typical applications for BCs are bioreactors, desalination units and humidifiers. Francis and Pashley investigated the use of a BC to determine the latent heat of aqueous salt solutions, suggesting that the high evaporation rate of BCs could be utilized for evaporative cooling of e.g. air conditioning units [25]. Their low complexity combined with high mixing and evaporation rates [26–28] make them a promising alternative to utilize the latent heat of the FC product water that is not subjected to the presented challenges of alternative water evaporative cooling solutions.

Nevertheless, previous investigations for the use of BCEs focus mainly on the increased liquid mixing and heat transfer caused by the turbulence from the bubble stream, e.g. in shell and tube heat exchangers [29,30], or the evaporation of water in desalination and humidification applications [26], [28], [31,32] rather than the evaporative cooling effect itself. Fundamental bubble heat and mass transfer investigations [33] and the desalination/humidifier studies found high heat and mass transfers with only minor impact of the water height.

To compare BCs of different sizes, normalized parameters are used to describe the respective gas (air) ($\dot{V}_a$) and liquid (water) volume flow rates ($\dot{V}_w$) through a given cross-sectional area (A_{column}), called superficial gas and liquid velocity, $v_{sf,g}$ (SGV) and $v_{sf,l}$, respectively. The resulting superficial gas and liquid velocities are defined at BC midpoint conditions and can influence the resulting bubble flow behavior [31], [33–35].

$$v_{sf,g/l} = \frac{\dot{V}_{a/w}}{A_{column}} \tag{1}$$

For compact cooling systems, the SGV needs to be increased as much as possible while maintaining high evaporation rates. Previous studies have, to the best of the author's knowledge, only investigated and shown the high evaporation efficiencies for SGVs of up to 0.3 m/s [32] for which mean bubble diameters stay roughly unchanged [36] and shown that the interfacial area, i.e. the bubble size dependent heat and mass exchange area between the bubbles and water, continues to increase up to 0.4 m/s [37]. Only for bioreactors, higher SGVs of up to 1 m/s have been reported [27].

The scaled down proof-of-concept of the BCE cooling approach presented in this study is investigated to prove its viability to supplement the heat rejection of the conventional radiator cooling system in heavy-duty FC trucks and overcome its thermal limitations. It is validated by theoretically predicting heat rejection rates in steady-state operating conditions. Higher superficial gas velocities than previously reported are investigated to reduce the cooling system size. A vehicle specific integration and packaging study has not been conducted but an estimated sizing has been derived based on the proof-of-concept limitations and steady-state full FC load operation of a verified heavy-duty truck model. Except for the horizontal water flow cooling investigated by Miyashita et al. for

power plants in Ref. [38], the authors are not aware of any prior investigations of a closed loop cooling system that utilizes a high volume air bubble stream to evaporatively cool an energy conversion system with ample availability of water, and none for BCEs in transport applications or combined with PEMFCs.

After presenting the state-of-the-art and motivation for bubble column evaporators as a supplemental cooling system in section 1, the BCE cooling concept and underlying heavy-duty FC truck model are presented in the following section 2, followed by the experimental proof-of-concept measurements and validation in section 3. Based on the findings from the proof-of-concept, the combined BCE and convectional cooling system performance and sizing for a heavy-duty FC truck is evaluated in section 4, followed by the summary and conclusion in section 5.

2. Bubble column evaporative cooling concept

Water produced in the electrochemical PEM fuel cell reaction of hydrogen and oxygen can be separated from the FC exhaust to be used for evaporation, utilizing the high latent heat of water to reject additional heat. In the following section, we present the underlying HD FC truck model as well as the redesign of the novel bubble column evaporator (BCE) cooling concept for FC vehicles, developed and presented in Ref. [24], showing promising heat rejection improvements compared to the conventional cooling system alone.

2.1. Heavy-duty fuel cell vehicle model

To identify the thermal limitations of conventional cooling systems in heavy-duty fuel cell electric vehicles (FCEV), a verified 44 t EU FC truck 0D/1D simulation model has been developed in Siemens Simcenter Amesim (version 2410). The propulsion system consists of two low-temperature PEMFC stacks with 328 kW total net power and a Li-ion battery to support in transient operation and store energy from regenerative braking. To substitute engine braking in the electric drivetrain, two braking resistors (BRs) reject additional heat into the FC cooling circuit. A single 0.9 m^2 radiator with an 850 mm fan has been implemented, maximizing the available space without a cabin redesign. The investigations reveal already severe thermal limitations of conventional cooling systems in HD FC trucks in a hill climb at 20 °C, which requires derating the FC power output to prevent overheating. This reduction in power leads to a significant slowdown of the vehicle. Additionally, the thermally limited BR power leads to performance limitations during downhill driving. The regenerative braking capabilities are further reduced if the battery is fully charged. We present further insights on the vehicle model and its thermal limitations in Refs. [24,39]. For the HD FCEV performance to be competitive with conventional diesel trucks, sufficient heat rejection needs to be achieved. Only marginal improvements on the radiator side are expected to be possible unless a significant reduction in pressure drop and thus fan power consumption could be achieved, since the validated radiator model already achieves high thermal efficiency. Alternatively, additional radiators could be placed on the vehicle, impacting its drag. Here the BCE cooling concept can be a promising alternative to achieve additional heat rejection and allow for sufficient FC power and avoid the most severe power limitations even at elevated temperatures.

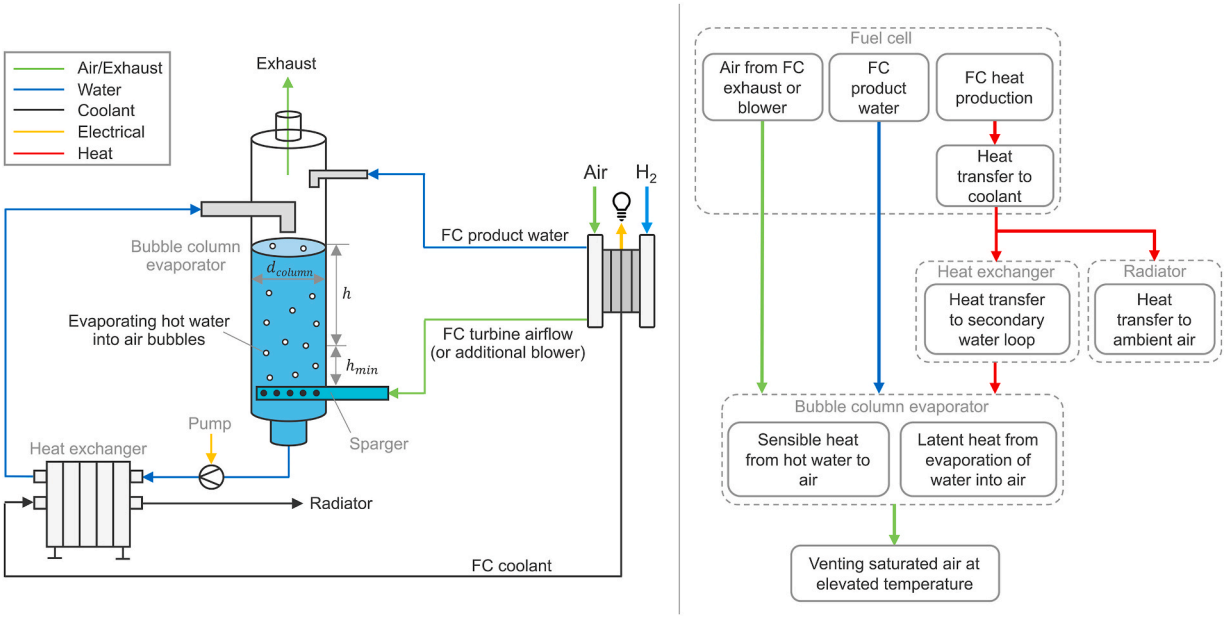

Fig. 1. Counterflow bubble column evaporative cooling system (left) and operating principle flowchart (right).

2.2. Bubble column evaporator design

A schematic of the counterflow BCE concept and an operating principle flowchart are shown in Fig. 1. To prevent the FC from overheating, the heat rejection of the radiator is supplemented by evaporating the FC product water in the presented BCE.

A counterflow plate heat exchanger transfers the heat from the FC coolant to the BCE water circuit which leads to a reduced radiator coolant inlet temperature that is outweighed by the additional evaporative heat rejection (see section 4). Previously in literature described liquid-to-liquid heat transfer limitations from submerged helical coils, see e.g. Ref. [28], are avoided by separating the water preheating from the bubble column evaporator. Inside the BCE, the FC exhaust air flow is injected through a sparger into the circulated hot water flow. This generates bubbles and removes heat via sensible heat up of the air and evaporation of water into the air stream, thereby cooling the water. By integrating the BCE downstream of the pressure recovery turbine of the fuel cell system (FCS), the energy recovery from the power input at the compressor is extended and thus further energy input is only required for the additional water pump. Alternatively, a separate blower could be used, potentially providing lower air inlet temperatures and relative humidities, more flexible control while avoiding potential impacts on the turbine backpressure control but requiring extra power input.

The bubble column itself consists of a lower section which contains the air inlet sparger above which a minimum water level of h_{min} is required, see section 3. Its diameter (d_{column}) depends on the superficial gas velocity that can be reached while still maintaining high evaporation rates, i.e. the amount of air that can eventually be run through a single unit. To operate the system for longer periods of time compared to the water production rate of the FC alone, a certain amount of water (h) needs to be stored which in turn depends on the desired available time of peak cooling. Additionally, a certain headroom is required to allow for the water to splash in the column and to house the water return and FC product water inlets. It can be designed as part of the exhaust if pressurization of the tank is avoided since increased pressure would reduce the water uptake in air. Finally, saturated exhaust air is vented at an elevated temperature and the cooled water circulated back to the heat exchanger.

2.3. Theoretical evaporative heat rejection rate

To compare the measured heat removal rate from the water flow presented in section 3.2 to the theoretically expected heat rejection from water evaporation, the following section presents the implemented method which is also used in the design study presented in Ref. [24] and section 4. The total evaporative heat rejection ($\dot{Q}_{evap,t}$) for steady-state operation is determined as the sum of sensible heat flow to the air ($\dot{Q}_{sens,a}$) and the latent heat of the evaporated water ($\dot{Q}_{lat,w}$) [26], [40,41]:

$$\dot{Q}_{evap,t} = \dot{Q}_{sens,a} + \dot{Q}_{lat,w} \tag{2}$$

with

$$\dot{Q}_{sens,a} = \dot{m}_{a,dry} \cdot \left(c_{p,a} \cdot \left(T_{evap} - T_{a,i}\right) + \omega_i \cdot c_{p,v} \cdot \left(T_{evap} - T_{a,i}\right)\right) \tag{3}$$

and

$$\dot{Q}_{lat,w} = \dot{m}_{w,evap} \cdot \Delta h_v\left(T_{evap}\right) \tag{4}$$

in which $\dot{m}_{a,dry}$ is the dry air mass flow rate, $c_{p,a}$ and $c_{p,v}$ the constant pressure specific heat capacities of air and vapor, respectively, T_{evap} the evaporator air outlet temperature which is assumed to be equal to the water bulk and thus evaporation temperature, $T_{a,i}$ the evaporator air inlet temperature, $\dot{m}_{w,evap}$ the evaporated water mass flow rate, Δh_v the temperature dependent vaporization enthalpy of water and ω_i the inlet absolute humidity. For the measurements presented in section 3, dried air is supplied by the facility compressor and assumed to have a relative humidity of 0%. For the vehicle scale system in section 4, a fully saturated FC exhaust air flow at 60 °C at 1.5 bar is assumed. In both cases the air is then assumed to be vented at full saturation of 100% relative humidity at bulk water temperature T_{evap}. The evaporated water mass flow rate is determined from the dry air flow rate and difference between inlet and outlet absolute humidity (ω_o):

$$\dot{m}_{w,evap} = \dot{m}_{a,dry} \cdot \left(\omega_o - \omega_i\right) \tag{5}$$

with the dry air mass flow being determined from the total (humid) air mass flow ($\dot{m}_a$):

$$\dot{m}_{a,dry} = \frac{\dot{m}_a}{1 + \omega_i} \tag{6}$$

and the absolute humidity generally defined for air as:

$$\omega = 0.622 \cdot \frac{\varphi_a \cdot p_{sat}(T_a)}{p_a - \varphi_a \cdot p_{sat}(T_a)} \tag{7}$$

with the relative humidity of air φ_a and water vapor saturation pressure p_{sat} which is determined as a function of the respective air temperature (T_a), valid for 0-100 °C:

$$p_{sat}(T_a) = 610.8 \cdot \exp\left(\frac{17.08085 \cdot T_a}{234.175 + T_a}\right) \; with \; T_a \; in \; °C \tag{8}$$

Since the investigations of Nikiforow et al. [28] and Abd-ur-Rehman et al. [32] as well as our proof-of-concept measurements indicate small sparger pressure drops, sufficient FC turbine outlet pressures to drive the system are expected and no theoretical investigation on air and water side pressure losses in the BCE have been conducted. Additionally, the low water height results in low hydrostatic pressures and impacts from the water flowing opposite on the rising air bubbles is expected to be negligible for the investigated conditions in this study $(v_{sf,l,max} = 0.021\ m/s)$ [35]. The air flow is simplified as pure air instead of oxygen depleted FC exhaust since the changes in properties are expected to be negligible with nitrogen as the major species in both cases. Furthermore, a perfectly insulated system and atmospheric sea level pressure at the sparger inlet and evaporator outlet are assumed.

3. Experimental proof-of-concept

To investigate the practical viability of the bubble column evaporative cooling concept, a proof-of-concept test bench has been built. The temperature difference between inlet and outlet water flow is measured to determine the average heat rejection rate from the water flow. No investigations of bubble size and behavior or gas holdup have been carried out. Furthermore, the challenging product water capture and condensation or measurement of inlet and outlet relative humidity as presented e.g. in Ref. [26] or [31] were not attempted at this proof-of-concept stage.

3.1. Proof-of-concept setup

Initially, a parallel flow layout similar to the concept design that we presented in Ref. [24] was built and tested. The large amount of water involved in the column and tank to also cover the water outlet (around 46 L) led to limited achievable air flow rates in the prototype due to shaking and spillage. Thus, the system was reconnected to a counterflow design as shown in Fig. 2, requiring significantly less water. In addition to the counterflow of air to water, the water flow now corresponds to the density driven separation of hot and cold water.

The schematic on the left side of Fig. 2 shows the layout of the test bench and the positioning of the sensors. Two mass flow controllers (MFCs) supply air in parallel to the air inlet system. The volume flow rate ($\dot{V}_a$) is measured on both sides, the inlet pressure (p_a) and temperature (T_a) only on one side. Air is injected 15 cm below the water surface and is then vented through the exhaust. For the sparger system, a symmetric pattern of 96 holes with 2 mm diameter on a 110 mm diameter surface has been used. The number and size of holes has been chosen to maximize the air flow area of the prototype sparger while reducing leakage into the sparger (compare [32]). Future iterations could also include different sparger designs since it influences the flow in the column [34,36], although the evaporation rate might not be affected [28,31]. The off-center air injection of the prototype sparger could further alter the bubble and water flow behavior and could be replaced by a more centralized air injection positioned lower in the BC.

The air inlet pipe into the BC has an inner diameter of about 48 mm. With a BC inner diameter of 0.194 m, reduced by the air inlet

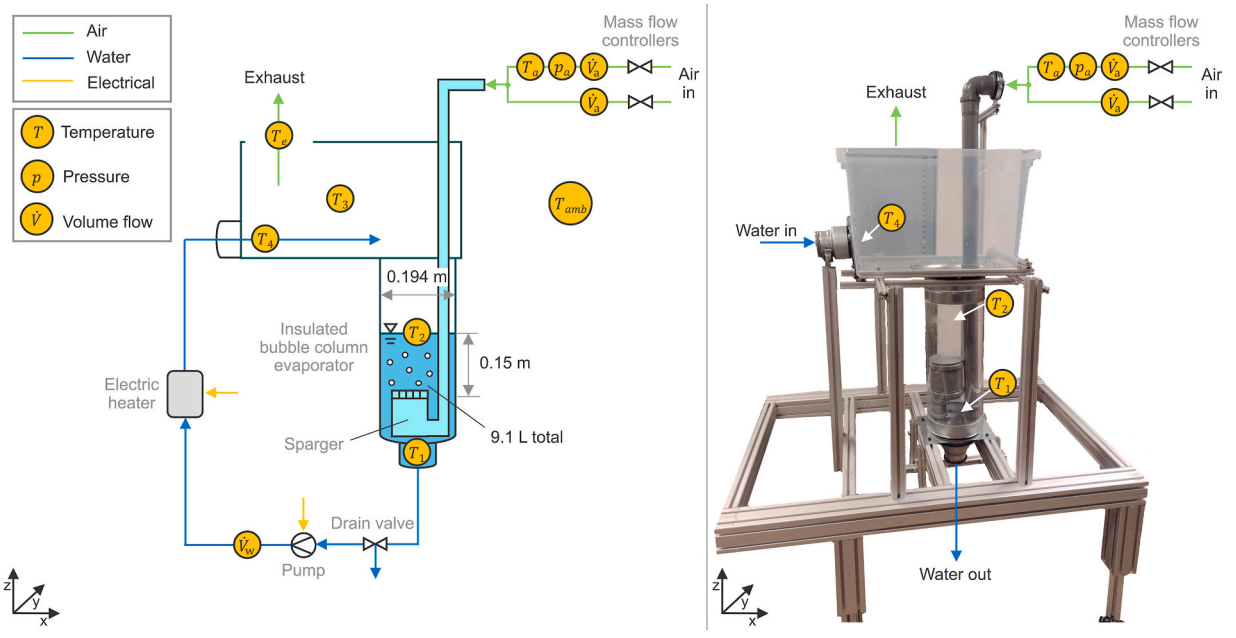

Fig. 2. Experimental counterflow setup schematic (left) and corresponding proof-of-concept rig without insulation (right).

pipe to an effective cross-sectional area of 0.18745 m, and the volume taken up by the air sparger, the total water volume at the start of each measurement is about 9.1 L. After passing through the water, the air temperature in the tank (T_3) and at the exhaust (T_e) are measured. Additionally, the ambient (T_{amb}) and water surface temperature (T_2) are measured. Temperature T_2 can only be used to monitor the bulk water temperature before the start of the measurement. As shown later, the water surface does not remain planar and the evaporation of water reduces the water level continuously. The heat rejection from the circulated water flow is determined from the temperature difference between the water inlet (T_4) and outlet temperature (T_1). A pump circulates the water volume flow ($\dot{V}_w$) and two electric heaters represent the FC heat load. Each of the presented steady-state measurements is conducted in three steps: (1) Filling water level to 15 cm above the sparger while circulating and heating the water to the respective setpoint, (2) start LabVIEW measurement and (3) start air flow and measure stabilized water inlet and outlet temperatures.

The average heat rejection from the water flow ($\dot{Q}_{w,avg}$) is determined by measuring the average temperature change ($T_{4,avg} - T_{1,avg}$) in the average water flow ($\dot{m}_{w,avg}$) during steady-state conditions:

$$\dot{Q}_{w,avg} = \dot{m}_{w,avg} \cdot c_{p,w} \cdot \left(T_{4,avg} - T_{1,avg}\right) \tag{9}$$

with the constant pressure specific heat capacity of water $c_{p,w}$. This heat rejection rate is later compared to the theoretically expected evaporative heat rejection rate ($\dot{Q}_{evap,t}$) determined in section 2.3 and used to develop the vehicle scale BCE cooling concept.

To reduce the losses to ambient, the column, tank and water inlet pipes were largely insulated. In the initial parallel design, the tank was used to store water and separate the bubbles from the water to prevent them from flowing to the pump. In the counterflow layout the tank only serves as the headroom to prevent water from spraying into the surrounding area. This could also be achieved by rebuilding the system with a higher column as shown in Fig. 1, which was not conducted in this proof-of-concept stage. The measurement equipment used is summarized in Table 1.

An average offset bias of around 12% has been found for the MFC setpoints in the measurement software by measuring the air flow in the chosen setpoints against a Venturi meter, likely caused by higher air densities at the pressurized MFC inlets. This offset has been corrected for the MFC measured air flow rates, resulting in a maximum of 35.84 g/s air flow rate which corresponds to an air volume flow rate of around 2000 L/min at average BCE operating temperatures, resulting in a superficial gas velocity of around 1.22 m/s with a superficial liquid velocity of around 0.021 m/s in the effective cross-sectional area.

The thermocouples have been calibrated at 20 and 85 °C, showing a spread of about 0.35 °C at resting conditions. The uncertainty in the water flow rate is determined based on an error of less than 1% FS given for the water flow sensor [42], an error of ±0.49% RD and ±0.46% FS for the data acquisition unit [43] and a 95% confidence level (1.96σ) of the measured value. With the repeatability of 2% between the five measurements presented for the maximum air flow rate (see section 3.2), the average square-root of the sum of squares (SRSS), see e.g. Ref. [44], for the heat rejection rate from the water flow ($\dot{Q}_{w,avg}$) is determined as ±7.5%. The correction of the air mass flow rate is based on the Venturi meter measurements for which the uncertainty is determined with the differential pressure measurement with an accuracy of 0.25 % RD [45] as well as uncertainty in the air density, discharge coefficient and geometric parameters of the Venturi meter itself [46,47]. Combined in the sensitivity-weighted SRSS provided in Ref. [47], the resulting air mass flow uncertainty is ±6.645%.

The operating points for the air and water flow rate have been chosen to scale according to the air to water flow ratios required at the vehicle level dimensioning, limited by the pump speed setpoints. By keeping similar flow ratios between the proof-of-concept test bench and vehicle scale study it can be investigated if the air flow in the opposite direction to the water could cause issues like e.g. blowing out water. For practical implementations of the BCE concept at large scale, further investigations are required to identify if its performance can be improved by changing the ratio between air and water flow rate e.g. to run higher water flow rates through the heat exchanger to improve its heat transfer rate or increasing the gas holdup of the column [35].

Fig. 3 shows the bubble column before and during a measurement, for visualization purposes without insulation.

On the left side, the BC is shown with 34 L/min of water circulation at time t_0 before the start of the measurement with indication of the temperature sensors positions. The images to the right show three consecutive moments in time ($t_1 - t_3$) with the maximum air flow rate of 35.84 g/s and 34 L/min water flow rate. The highly turbulent flow leads to water splashing and swirling mixing of the water. Thus, the water surface becomes highly amorphous. It was not observed that larger bubbles flow into the water outlet or that the air

Table 1
Measurement equipment overview.

Measurement/Device	Model	Range
Temperature	Thermocouple, type K, d = 1.5 mm	−40-1100 °C
Air flow rate	Bronkhorst Mass-Stream D-6471	0-1000 L/min
Air flow rate	Brooks Model 5853	0-600 L/min
Water flow rate	ifm SV7050	5-85 L/min
Pressure	Wika S-10	0-6 bar
Data acquisition (T)	National instruments NI-9212	±78.125 mV
Data acquisition ($p, \dot{V}$)	National instruments NI-9203	0-20 mA
Water pump	Lowara ecocirc XL 32-100	max. 10.7 m^3/h
Heater (2x)	RELEK RK71E	9 kW (each)
Manometer	Furness Controls FCO510	0-200 Pa

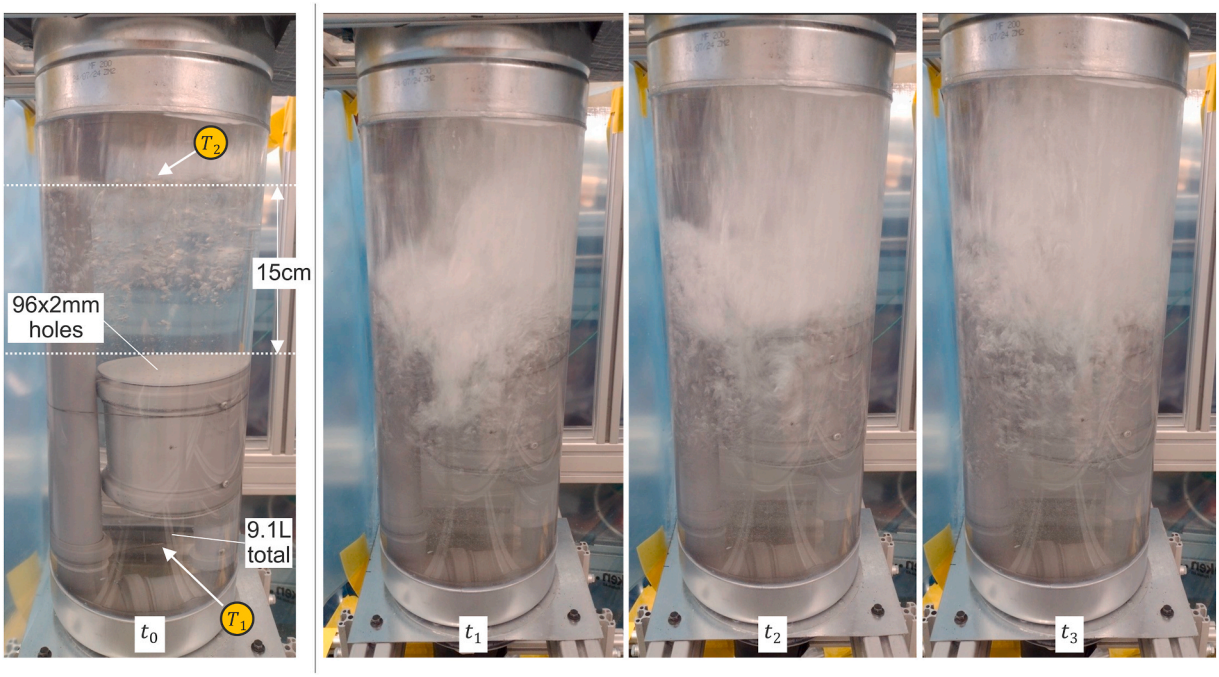

Fig. 3. 34 L/min water flow rate at t_0 (left), 35.84 g/s air and 34 L/min water flow for three consecutive moments in time $t_1 - t_3$ (right), without insulation.

flow blows out water directly.

3.2. Measurement results

The measurement results for one measurement at maximum air and water flow rate are shown in Fig. 4.

After a stabilization phase that follows the start of the air flow provided by the two MFCs, the average air inlet and ambient temperature are 17.1 °C and 18.3 °C, respectively. The heaters provide an average water inlet temperature of around 59.67 °C at 34.2 L/min water flow rate that gets cooled down to an average water outlet temperature of 54.42 °C, leading to an average heat rejection rate ($\dot{Q}_{w,avg}$) of around 12.3 kW. The measured temperatures of the air (flow) inside the tank (T_2 and T_3) and at the air outlet (T_e) are close to the water temperature measured at the bottom water outlet (T_1), suggesting that the assumption of high mixing rates and evaporation at bulk water temperature are justified. Due to the splashing and the highly amorphous water surface, measuring the actual evaporation temperature at the water surface was not possible.

The water level reduction has been measured with a ruler, reducing by roughly 7 cm in this measurement which corresponds to

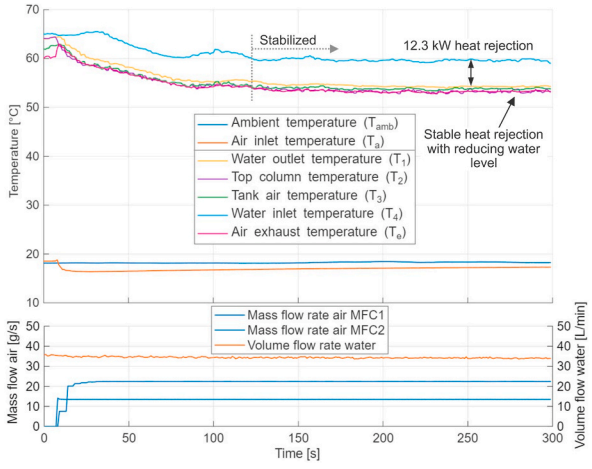

Fig. 4. Measurement result at maximum flow rates of 35.84 g/s air (1.22 m/s SGV) and 34.2 L/min water.

around 1.9 kg of evaporated water. Due to the uncertainty of the manual reading with imposed water flow rates and the higher evaporation rate during the initial phase of the measurement compared to the average stabilized phase, the measured and theoretically expected average water evaporation rate cannot be directly compared. Evaporating 1.9 kg in the time of the measurement would result in an average water evaporation rate of 6.3 g/s and a latent heat rejection rate of around 15 kW, exceeding the measured heat removal rate from the water. This indicates that some water could be carried out of the BCE in the form of droplets rather than evaporating, effectively reducing the water utilization rate. But based on the theoretically expected water evaporation rate of around 4 g/s, it is still likely to be higher than 60%. Further measurements of the large scale design with water capture and accurate water level measurements are required to determine the water utilization rate and if parts of the non-evaporating droplets can be returned to the column from the headroom section and exhaust pipe.

Despite reducing water level, the measured temperature difference is stable, suggesting that lower water levels should achieve similar evaporation efficiencies due to high heat and mass transfer rates. Thus, a minimum required water level at these high air flow rates could be lower than the investigated 15 cm. The inlet air pressure measurements (not shown) at the MFCs indicate that the pressure increase can be attributed to the air inlet hoses and that the contribution of the sparger and water column are negligible in comparison. This suggests only a small impact on the FC exhaust backpressure for the intended FCS integration.

To investigate the repeatability of the measurement, five measurements with stabilized measurement times between 100 and 375 s are shown Fig. 5, including the result from Fig. 4 as measurement 5.

The resulting average heat rejection is repeatable within 2% of the average heat rejection of 12.5 kW. In these five measurements, the average temperature difference varies between 5.2 and 5.6 °C and water flow between 32.8 and 35.4 L/min. The difference in water flow rate is compensated for by a (small) increase or reduction in the resulting temperature difference, leading to similar heat rejection rates. Furthermore, the measured heat rejection rates are insensitive to the air inlet and ambient temperatures which varied between 16.9-18.6 °C and 17.4-20.2 °C, respectively.

3.3. Validation

Seven air flow rates of 5.81-35.84 g/s (0.2-1.22 m/s SGV) with water flow rates of 10-34 L/min have been investigated to determine the behavior at different operating points and to estimate if an upper limit of achievable heat rejection was reached. A Monte Carlo sensitivity analysis showed that the chosen assumptions for the evaporative heat rejection ($\dot{Q}_{evap,t}$) strongly influence the resulting mean and uncertainty values of the theoretical calculations, especially the air mass flow rate and relative humidity at the outlet. Therefore, a comparison between the expected best- and worst-case is chosen to show the range of the anticipated results. Respective changes for the best- and worst-case are shown in Table 2, either as a direct value for an assumption or as a relative change of a measured nominal value.

The variation of the pressure is based on the expected pressure variation of the measurement location at sea level as well as the additional increase at the air inlet (sparger outlet) from the hydrostatic pressure of the 15 cm water column. The result is insensitive to the hydrostatic pressure due to low or non-existent water content in the inlet air and furthermore expected to be reduced in practice since the lift from the high air flow rate causes splashing which means that no full water column is located above the sparger inlet continuously. In Fig. 6, the comparison between the measured average heat rejection from the water flow ($\dot{Q}_{w,avg}$) and the theoretically

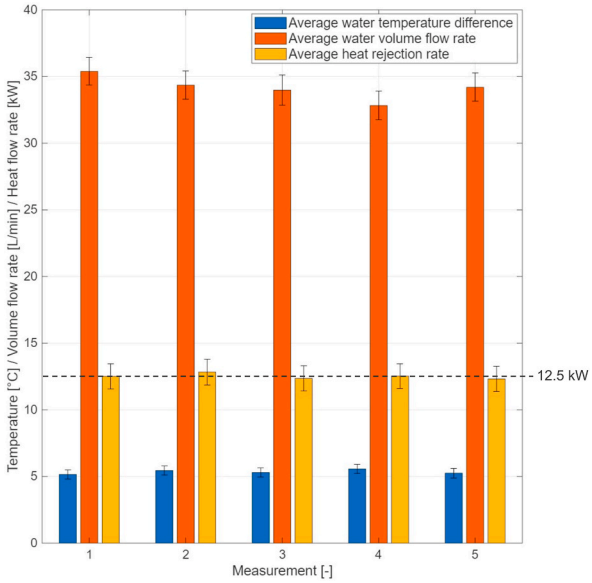

Fig. 5. Maximum air flow rate measurement repeatability.

Table 2
Theoretical calculation assumption range for evaporative heat rejection.

Parameter	Type	Nominal	Worst-case	Best-case
Evaporation temperature	Measured	$T_{evap} = T_1$	−0.35 °C (<-1%)	+0.35 °C (<+1%)
Air inlet temperature	Measured	$T_{a,i}$	+0.35 °C (+2%)	−0.35 °C (−2%)
Air mass flow rate	Measured	$\dot{m}_a$	−6.645%	+6.645%
Inlet relative humidity	Assumed	0%	10%	0%
Outlet relative humidity	Assumed	100%	95%	100%
Air inlet pressure (sparger)	Assumed	1.013 barA	1.003 barA (−1%)	1.037 barA (+2.4%)
Air outlet pressure	Assumed	1.013 barA	1.023 barA (+1%)	1.003 barA (−1%)

determined evaporative heat rejection rate ($\dot{Q}_{evap,t}$) for the worst-, nominal and best-case are shown for the seven different operating points.

For all air flow rates, the best and nominal theoretical cases are within or close to the uncertainty of the measured heat rejection from the water flow. It should be noted that at the lower air flow rates, the heater operation is less continuous due to hysteresis, causing the water inlet and outlet temperatures to oscillate periodically around their mean value. With the exponential increase of saturation pressure with temperature this might affect the average heat rejection rate, although especially for the lower air flowrates, measured and best-to worst-case results are matching closely.

For higher air flow rates, it is suspected that the splashing of the water leads to higher levels of losses which increase the gap between the measurement and theoretical cases, although the best-case assumptions still overlap with the uncertainty of the water flow heat rejection measurement. This suggests that the expected full saturation at the outlet is reached. The continued increasing trend in the average water heat rejection suggests that an upper limit of achievable heat rejection might not be reached at the maximum air flow rate and thus higher air flow rates with continued high heat rejection rates could be possible in the same sized system.

Unlike the measured heat rejection from the water flow ($\dot{Q}_{w,avg}$), the calculation of the theoretical evaporative heat rejection ($\dot{Q}_{evap,t}$) does not include losses to ambient. To investigate the losses, three additional measurements were conducted: (1) In a 500 s cooldown measurement with around 64 °C initial water temperature and no air or water flow, it was found that the insulated BC only loses around 100 W. (2) Additionally, no measurable temperature difference higher than the sensor uncertainty between water inlet (T_4) and outlet (T_1) was observed when circulating 35 L/min water (without airflow) at 45 and 64 °C, respectively. At this water flow rate, a loss of around 815 W would be within the 0.35 °C spread of the temperature sensors and thus within the measurement uncertainty and not directly visible. Including this loss would lead to an increase of around 7.6% of the expected theoretical evaporative heat rejection at maximum air flow rate. (3) To evaluate if additional losses occur in the flow section of the tank from the water inlet to the BC (T_4 to T_2), the water inlet pipe has been positioned directly above the column, similar to the layout shown in Fig. 1. The result is included as measurement 4 in Fig. 5 and shows no significant difference to the other measurements, indicating that the measurement setup with the additional tank section does not impact on the overall losses measurably.

Further measurements in a large scale system with measurement of inlet and outlet conditions are required to identify relevant losses, the BCE performance at the required high air and water flow rates and to validate dynamic BCE models which take transient effects into account. More temperature measurement points could provide further detail of the temperature distribution within the complex flow field of the BC and exhaust, especially if the column size and volume are significantly increased. Measuring higher water temperatures was not possible in this proof-of-concept stage due to material limitations but operating closer to the FC operating temperature and supplying air at FC exhaust conditions would allow for a closer validation of the developed concept.

In the next section, the performance and sizing of the BCE on a HD FC truck scale are evaluated based on the findings of the proof-of-concept measurements.

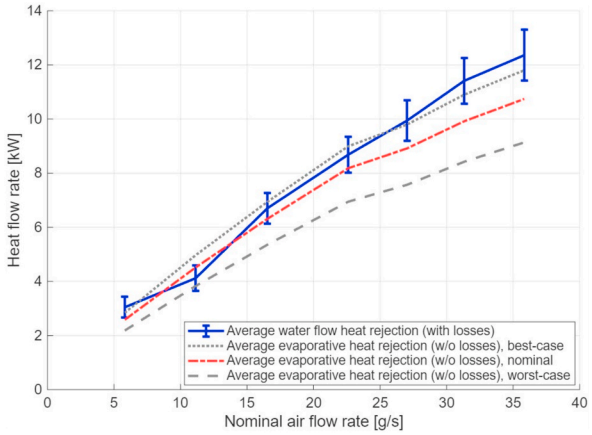

Fig. 6. 5.81-35.84 g/s air flow (0.2-1.22 m/s SGV) with 10-34 L/min water flow rate heat rejection comparison.

4. Heavy-duty FCEV cooling performance and sizing

In the following section, the highly integrated solution utilizing the FC turbine exhaust is investigated to evaluate the performance potential of the BCE on a heavy-duty vehicle level scale. Fig. 7 shows the performance matrix of the designed system, depicting the BCE heat rejection with water evaporation rates as a function of the evaporation and FC outlet temperature (left) and normalized combined heat rejection rate of the BCE and radiator as well as the available operating time of the system based on exemplary 50 kg water storage (right). Compared to our previous study [24], the assumptions of the available air flow rate from the FCS have been adjusted to closer match the vehicle FC model, the plate heat exchanger performance is now based on the data provided by Ref. [48] for a unit matching the expected dimensioning and the evaporator outlet is assumed to be fully saturated based on the findings from the proof-of-concept measurements.

At 20 °C ambient temperature, 85 km/h and full FC load with 315 g/s fully saturated FC exhaust air flow at 1.5 bar and 27 g/s water production rate, sufficient heat rejection is achieved for around 23 min with a total BCE heat rejection rate of around 153 kW, evaporating around 64 g/s of water. The required FC outlet temperature and water evaporation temperature are around 83 °C and 72 °C, respectively. Longer operating times can be achieved by storing more water. The heat rejection rate increases exponentially with the evaporation temperature due to the exponential increase in saturation pressure with temperature and thus water uptake potential [49], compensating for the reduced radiator coolant inlet temperature. If the water evaporation rate is equal or lower to the FC water production rate, the system can be operated continuously (≥100 min). However, at the maximum shown heat rejection at high FC operating temperatures and thus water evaporation rates, the operating time reduces to less than 2 min. Thus, the ideal operating point for the given assumptions is located on the grey plane at the lowest FC outlet temperature that allows for full heat rejection, given that the FC operating temperature limits are respected. While real system could not exceed the maximum heat production of the FCS, the results are not cut off to show potential operating points in which e.g. the fan power could be reduced due to excess BCE performance. The integration of a dynamic model of the BCE into the verified Amesim HD FC truck model is currently under development to evaluate its performance in typical and challenging driving scenarios.

The combined heat rejection at 20 °C improves the cooling capabilities by more than 40% compared to directly running the FC coolant at this temperature to the conventional radiator which alone cannot provide sufficient heat rejection to allow for full FC load. To achieve full FC heat rejection at elevated temperatures, the operation of the combined system needs to be adjusted. For example, the radiator heat rejection rate can be improved by allowing higher fan speeds, requiring increased fan power. The BCE operation could be improved e.g. by increasing the air flow rate through increased FC stoichiometry or bypassing the cathode as well as operating the FC at higher temperatures (<90 °C) which would require careful calibration with the FC performance and lifetime. Additionally, a larger plate heat exchanger could be used. Further potential improvements to the concept have been discussed in Ref. [24]. Nevertheless, at 35 °C ambient temperature, the same operating point provides more than 80% of the required total heat rejection, allowing for significantly improved vehicle performance and improving by more than 50% compared to running the coolant from the FC directly to the radiator. At 45 °C, more than 70% of the required heat rejection is achieved which is an improvement of more than 70% compared to the conventional cooling system.

The ideal operating point resulting from the design matrix shown in Fig. 7, the assumptions for the full-load FC operating point and the BCE sizing based on the presented experimental limitations, i.e. superficial gas and liquid velocity as well as air to water flow ratio, are summarized in Fig. 8 (not to scale).

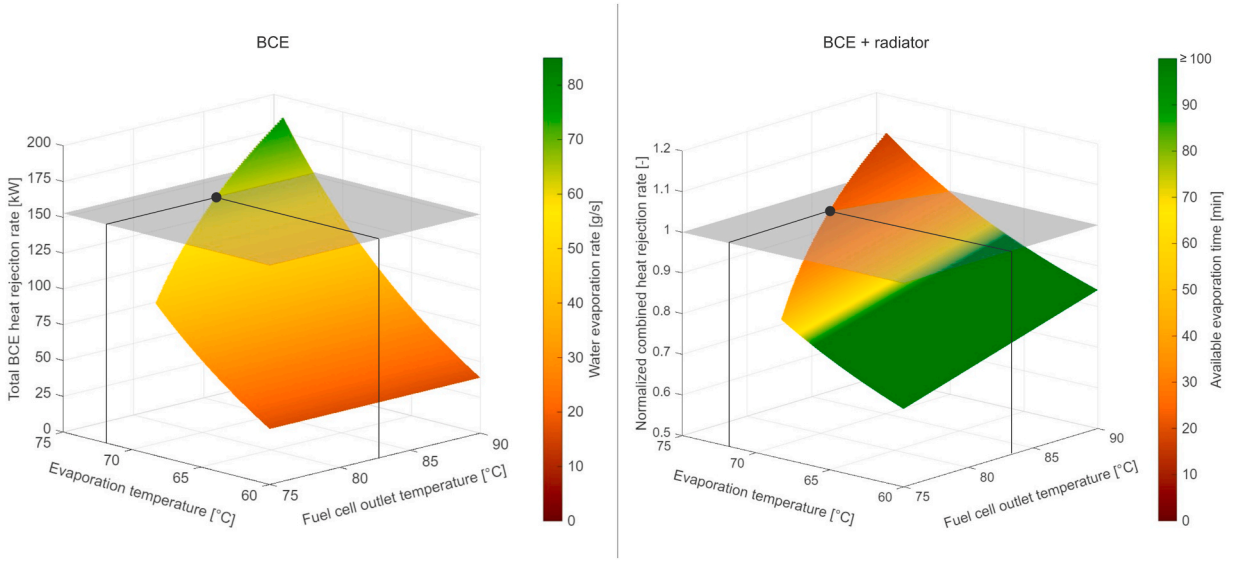

Fig. 7. Performance envelope of the BCE showing heat rejection rate and water evaporation rate (left) and BCE plus radiator combined normalized heat rejection rate and resulting operating time (right) at 20 °C ambient, 85 km/h, full FC load with 27 g/s water production.

The FC product water that refills the storage might enter the column at FC operating temperature if no heat is lost in the water separator. Assuming a water production rate of 27 g/s at 83 °C that is cooled to 72 °C requires an additional heat removal of around 1.2 kW, less than 1% of the expected evaporative heat rejection rate. A bypass might be required in practical implementations to allow running the cooling system without BCE support and control the air mass flow into the BCE. Based on the parameterization data of the FC coolant pump [50], the modelled power consumption is expected to be around 400 W at 5.2 kg/s. To evaluate the effectiveness of the developed BCE cooling system, the ratio between heat removal and required power input as defined in Ref. [3] is determined:

$$Effectiveness = \frac{heat\ removal\ rate}{electrical\ power\ consumed\ by\ fan, blower\ or\ pump} \tag{10}$$

The conventional cooling system of the verified HD FC truck model individually achieves a ratio of around 19 at 20 °C ambient temperature, 85 km/h and full FC load, similar to the investigations presented e.g. in Ref. [51]. The presented BCE individually achieves a ratio of around 383 when operated with the FC exhaust (no additional power for air flow) and the additional water pump, highlighting the potential of utilizing the latent heat of water. As a result, the combined BCE with radiator effectiveness improves to a ratio of around 27.

Based on the presented measurements, the sizing of the BCE on HD FCEV scale can be estimated. Running the total full-load FC exhaust air flow rate through a single BCE unit at the currently proven maximum SGV would result in a column diameter of around 0.56 m. Storing 50 kg of water for peak cooling requires a 0.2 m water column (h) above an assumed water level of 0.2 m to house the sparger and provide a minimum water level (h_{min}) of 5 cm above the sparger. This water column with a height of 0.4 m would continue to result in low hydrostatic pressure and the total weight of the water stored in the BCE would be around 100 kg. Assuming 5 mm steel walls and a headroom of around 0.4 m, the BCE itself would be around 0.8 m high and weigh around 76 kg while the chosen plate heat exchanger and pump weigh around 38.5 kg [48] and 7 kg [50], respectively. Neglecting the weight of the connectors, pipes, valves, sparger and water volume in the pipes, the total system weight is estimated to be around 221.5 kg. If the air flow rate through a single BCE could be increased further, more compact cooling units can be designed. The final size of individual BCE solutions depends on the vehicle and FC specific performance targets, i.e. desired operating duration and heat rejection supplementation, so that the final BCE could be smaller than the preliminary results of this study and thus closer in size to the proof-of-concept. It might also be possible to design the BCE in a custom shape to fit the available space rather than being round, as long as key parameters like the SGV, stored amount of water, uniform air injection with free rising paths and prevention of tank pressurization are respected.

The resulting temperature and water content increase of the air flow are shown in Fig. 9 for the proof-of-concept nominal case at maximum air flow rate (red) and the vehicle scale conditions (blue dashed).

To show both processes in the same graph at 1 atm, the relative humidity at the FC outlet has been adjusted to the corresponding water content at full saturation at 1.5 bar. The psychrometric chart highlights the potential of evaporative cooling due to the exponential increase in water uptake with increasing temperature derived from equations (2)–(9).

It is worth noting that the performance of the BCE itself is not affected by the ambient air temperature if sufficient insulation is provided and improves at higher altitudes due to the increased water uptake at lower ambient pressures. The optimal operating point of the system thus requires a balance between the FC operation, desired heat rejection of the combined system, auxiliary power losses and available amount of water for the evaporation. In a real vehicle, additional practical challenges like G-forces, start-up procedures, vibration, noise and freezing conditions need to be considered, requiring further testing under realistic vehicle conditions in future

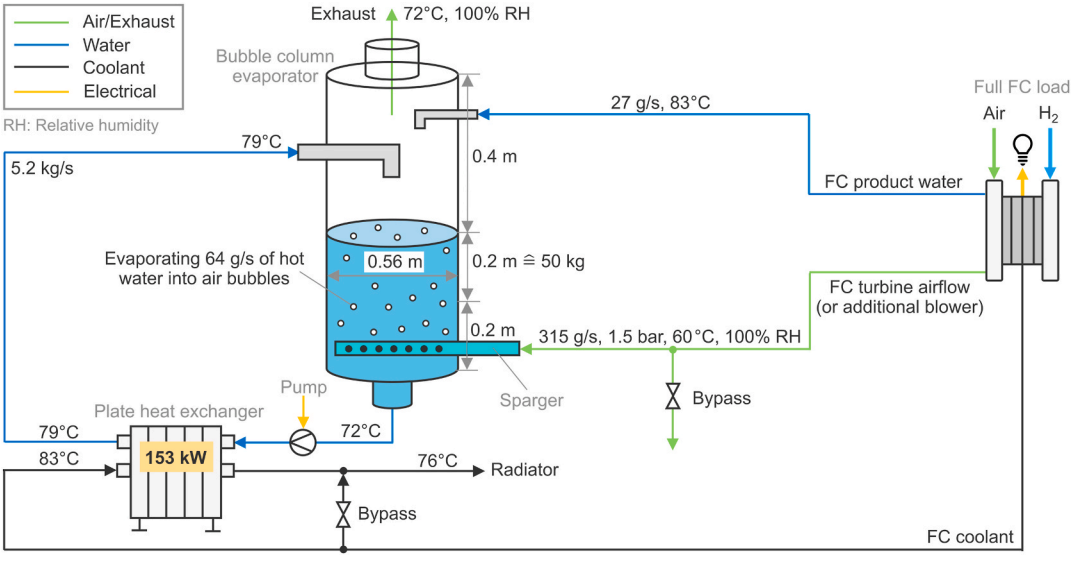

Fig. 8. Counterflow bubble column evaporative cooling system with determined operating conditions for full FC load at 20 °C ambient and 85 km/h and estimated sizing (not to scale).

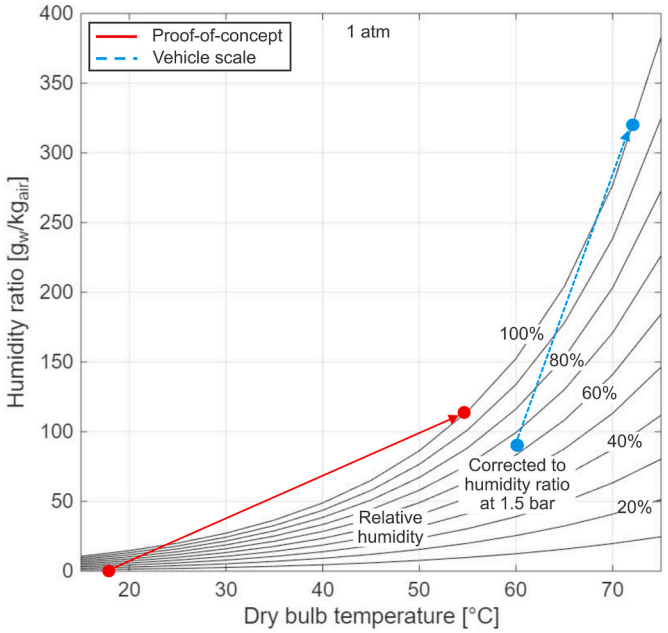

Fig. 9. Psychrometric chart for proof-of-concept (nominal maximum air flow rate) and vehicle scale system at full FC load.

investigations. Like for radiator spray-on solutions, liquid water draining might be required to avoid freezing [52], although likely only necessary at longer periods of parking at freezing conditions because otherwise the input of warm FC product water as well as the circulation of coolant and water add heat to the BCE system. Combined with predictive vehicle control, the stored and thus drained water mass in cold conditions could be held small since cold ambient temperatures mitigate cooling limitations. In case the pure FC product water that is used in the BCE could get contaminated with e.g. particles, a filter can be added to the secondary water loop. Suitable, corrosion-free materials need to be chosen to ensure durability. Unlike water spray-on radiator solutions which can lead to water injection into the underhood of the vehicle, only the amount of water vapor in the vented exhaust is increased in addition to the already saturated cathode exhaust.

5. Summary and conclusion

We have presented a novel counterflow bubble column evaporative cooling concept to utilize the FC product water for additional heat rejection and proved its viability in a proof-of-concept test bench, achieving high steady-state heat rejection rates which can be predicted with theoretical evaporation calculations. A superficial gas velocity of 1.22 m/s was reached, showing high heat rejection rates at significantly higher SGVs than previously presented in literature. The measurements suggest that even higher air flow rates might be possible in the same unit size, potentially allowing more compact units. The required air flow can be utilized from the fuel cell system in a highly integrated solution and vented through the exhaust.

The concept could complement the insufficient heat rejection of a conventional truck radiator cooling system at 20 °C ambient temperature with around 153 kW, achieving full heavy-duty truck PEMFC power for 23 min with 50 kg of useable water stored. This corresponds to an increase of over 40% over the conventional radiator cooling system at 85 km/h while requiring only 400 W for the additional water pump and not affecting the vehicle's drag. At elevated ambient temperatures of up to 45 °C, improvements of more than 70% could be achieved but operational adjustments or supplying the air flow by a separate blower might be required to provide sufficient combined BCE and radiator heat rejection.

The BCE concept benefits from low complexity and is especially suitable for fuel cell vehicles due to onboard water production, making it potentially viable for other fuel cell heavy-duty applications like planes, trains, tractors or ships. Further advantages for the thermal management of heavy-duty FCEVs that could be achieved are.

- Operating the BCE also during part-load driving can further reduce the fan power consumption throughout the driving operation.
- With atmospheric bubble column evaporator outlet conditions, the water uptake and thus heat rejection rates of the system improve with decreasing ambient pressures at higher altitudes.
- Potential challenges that can arise in radiator spray-on solutions like increased radiator fouling, channel blocking and water injection into the underhood compartment are avoided.
- The stored water thermal mass can buffer heat spikes from the braking resistors or fuel cell while radiator and evaporative heat rejection ramp up.

- Complementing the established conventional truck radiator system in existing truck platforms reduces the need for structural redesigns.

Further investigations at higher air flow rates and temperatures with an improved test bench setup are required to fully validate the theoretical assumptions, investigate water utilization rates and determine the limitations and sizing of the concept. A dynamic model of the bubble column evaporator is currently under development to be fully integrated into the verified heavy-duty fuel cell truck Amesim model to investigate its performance during typical and challenging driving operations.

CRediT authorship contribution statement

Christian Boßer: Writing – original draft, Visualization, Validation, Software, Methodology, Investigation, Formal analysis, Data curation, Conceptualization. **David Sedarsky:** Writing – review & editing, Supervision, Resources, Project administration, Funding acquisition.

Declaration of competing interest

The authors declare that they have no known competing financial interests or personal relationships that could have appeared to influence the work reported in this paper.

Acknowledgment

The Competence Centre TechForH2 is hosted by Chalmers University of Technology and is financially supported by the Swedish Energy Agency (P2021-90268) and the member companies Volvo, Scania, Siemens Energy, GKN Aerospace, PowerCell, Oxeon, RISE, Stena Rederier AB, Johnson Matthey and Insplorion.

The authors would like to thank Robert Buadu, Isak Jonsson, Valentin Vikhorev and Valery Chernoray at the Department of Mechanics and Maritime Sciences at Chalmers University for the support on the experimental investigations.

Data availability

The data that has been used is confidential.

References

[1] M. Beigtan, M. Gonçalves, B.M. Weon, Heat transfer by sweat droplet evaporation, Environ. Sci. Technol. 58 (15) (Apr. 2024) 6532–6539, https://doi.org/10.1021/acs.est.4c00850.
[2] K. Inthavong, D.F. Fletcher, M. Khamooshi, S. Vahaji, H. Salati, Wet surface wall model for latent heat exchange during evaporation, Int. J. Numer. Methods Biomed. Eng. 38 (4) (2022) e3581, https://doi.org/10.1002/cnm.3581.
[3] R.P. O'Hayre, S.-W. Cha, W.G. Colella, F.B. Prinz, Fuel Cell Fundamentals, third ed., John Wiley & Sons Inc, Hoboken, New Jersey, 2016.
[4] G. Zhang, S.G. Kandlikar, A critical review of cooling techniques in proton exchange membrane fuel cell stacks, Int. J. Hydrogen Energy 37 (3) (Feb. 2012) 3, https://doi.org/10.1016/j.ijhydene.2011.11.010.
[5] D.A. Cullen, et al., New roads and challenges for fuel cells in heavy-duty transportation, Nat. Energy 6 (5) (Mar. 2021) 5, https://doi.org/10.1038/s41560-021-00775-z.
[6] M. Nöst, C. Doppler, M. Klell, A. Trattner, Chapter 7 - thermal management of PEM fuel cells in electric vehicles, in: D. Watzenig, B. Brandstätter (Eds.), Comprehensive Energy Management - Safe Adaptation, Predictive Control and Thermal Management, Springer International Publishing, Graz, Austria, 2018, pp. 102–121, https://doi.org/10.1007/978-3-319-57445-5, in SpringerBriefs in Applied Sciences and Technology.
[7] K. Mayr, et al., Systemvergleich zwischen Wasserstoffverbrennungsmotor und Brennstoffzelle im schweren Nutzfahrzeug, E-Mobil BW GmbH – Landesagentur Für Neue Mobilitätslösungen Automot. Baden-Württ. Stuttg., 2021 [Online]. Available: https://www.e-mobilbw.de/fileadmin/media/e-mobilbw/Publikationen/Studien/e-mobilBW-Studie_H2-Systemvergleich.pdf.
[8] J. Linderl, J. Mayr, M. Hütter, R. Döbereiner, Optimized fuel cell drive for long-haul trucks, ATZheavy Duty Worldw. 14 (1) (Mar. 2021) 38–43, https://doi.org/10.1007/s41321-021-0407-5.
[9] Y. Huang, X. Xiao, H. Kang, J. Lv, R. Zeng, J. Shen, Thermal management of polymer electrolyte membrane fuel cells: a critical review of heat transfer mechanisms, cooling approaches, and advanced cooling techniques analysis, Energy Convers. Manag. 254 (Feb. 2022) 115221, https://doi.org/10.1016/j.enconman.2022.115221.
[10] A. Baroutaji, et al., Advancements and prospects of thermal management and waste heat recovery of PEMFC, Int. J. Thermofluids 9 (Feb. 2021) 100064, https://doi.org/10.1016/j.ijft.2021.100064.
[11] A. Fly, Thermal and water management of evaporatively cooled fuel cell vehicles. Thesis for the Degree of Doctor of Philosophy, Loughborough University, Loughborough, England, 2015.
[12] E.J. Choi, J.Y. Park, M.S. Kim, Two-phase cooling using HFE-7100 for polymer electrolyte membrane fuel cell application, Appl. Therm. Eng. 148 (Feb. 2019) 868–877, https://doi.org/10.1016/j.applthermaleng.2018.11.103.
[13] S.C. Kim, J.P. Won, Y.S. Park, T.W. Lim, M.S. Kim, Performance evaluation of a stack cooling system using CO2 air conditioner in fuel cell vehicles, Int. J. Refrig. 32 (1) (Jan. 2009) 70–77, https://doi.org/10.1016/j.ijrefrig.2008.07.003.
[14] S. Lee, M.S. Kim, Stack cooling system coupled with secondary heat pump in fuel cell electric vehicles, Energy Convers. Manag. 284 (May 2023) 116961, https://doi.org/10.1016/j.enconman.2023.116961.
[15] M. Reichler, Theoretische Untersuchungen zur Kühlleistungssteigerung durch innovative Kühlsysteme für Brennstoffzellen-Elektrofahrzeuge. Abhandlung Doktor-Ingenieur (Dr.-Ing.), Universität Stuttgart, Stuttgart, 2009 [Online]. Available: https://elib.uni-stuttgart.de/server/api/core/bitstreams/6d749339-0633-4f10-a135-a3bbc548069c/content.
[16] N. Philip, P.C. Ghosh, A generic sizing methodology for thermal management system in fuel cell vehicles using pinch analysis, Energy Convers. Manag. 269 (Oct. 2022) 116172, https://doi.org/10.1016/j.enconman.2022.116172.

[17] S. Swathi, A.S. Oberoi, R.K. Singla, Utilizing phase change materials for proton exchange membrane fuel cell cooling: a review, Environ. Prog. Sustain. Energy (Mar. 2025) e14596, https://doi.org/10.1002/ep.14596.
[18] M. Striednig, M. Cochet, P. Boillat, T.J. Schmidt, F.N. Büchi, A model based investigation of evaporative cooling for polymer electrolyte fuel cells – stack level analysis, J. Power Sources 517 (Jan. 2022) 230706, https://doi.org/10.1016/j.jpowsour.2021.230706.
[19] T. Rudolf, T. Schurmann, S. Schwab, S. Hohmann, Toward holistic energy management strategies for fuel cell hybrid electric vehicles in heavy-duty applications, Proc. IEEE 109 (6) (Jun. 2021) 6, https://doi.org/10.1109/JPROC.2021.3055136.
[20] R. Prabakaran, M. Mohamed Souby, J. Liu, S. Chul Kim, Thermal performance of a stack cooling radiator coupled with spray cooling for the future fuel cell electric vehicles, Appl. Therm. Eng. 246 (Jun. 2024) 122975, https://doi.org/10.1016/j.applthermaleng.2024.122975.
[21] R. Prabakaran, M.M. Souby, J. Liu, S.C. Kim, Dynamic performance of a fuel cell stack radiator coupled with low pressure drizzling cooling and intermittent flow strategies, Int. J. Heat Mass Tran. 235 (Dec. 2024) 126161, https://doi.org/10.1016/j.ijheatmasstransfer.2024.126161.
[22] D.K. Lee, D.S. Kim, H.S. Byun, H.S. Kang, Y.H. Shin, H.S. Lee, Maximizing FCEV stack cooling performance: developing a performance prediction model based on machine learning for evaporative cooling radiator. Presented at the WCX SAE World Congress Experience, Detroit, Michigan, United States, Apr. 2024, https://doi.org/10.4271/2024-01-2586, 2024-01–2586.
[23] J. Konrad, C. Varlese, R. Krizan, C. Junger, P. Hofmann, C. Mayer, Fuel cell electric tractor FCTRAC: powertrain, thermal system, hydrogen storage, and performance, Agric. Eng. 79 (3) (Aug. 2024) 3, https://doi.org/10.15150/AE.2024.3314.
[24] C. Boßer, D. Sedarsky, Bubble column evaporative cooling for PEMFC thermal management in heavy-duty vehicles. Presented at the 10th Thermal and Fluids Engineering Conference (TFEC), Begel House Inc., 2025, https://doi.org/10.1615/TFEC2025.mes.055991.
[25] M.J. Francis, R.M. Pashley, Application of a bubble column for evaporative cooling and a simple procedure for determining the latent heat of vaporization of aqueous salt solutions, J. Phys. Chem. B 113 (27) (Jul. 2009) 27, https://doi.org/10.1021/jp901801k.
[26] E. Eder, S. Hiller, D. Brüggemann, M. Preißinger, Characteristics of air–liquid heat and mass transfer in a bubble column humidifier, Appl. Therm. Eng. 209 (Jun. 2022) 118240, https://doi.org/10.1016/j.applthermaleng.2022.118240.
[27] B. Guieysse, G. Quijano, R. Muñoz, Airlift bioreactors, in: Comprehensive Biotechnology, Elsevier, 2011, pp. 199–212, https://doi.org/10.1016/B978-0-08-088504-9.00095-7.
[28] K. Nikiforow, J. Ihonen, T. Keränen, H. Karimäki, V. Alopaeus, Modeling and experimental validation of H2 gas bubble humidifier for a 50 kW stationary PEMFC system, Int. J. Hydrogen Energy 39 (18) (Jun. 2014) 9768–9781, https://doi.org/10.1016/j.ijhydene.2014.04.058.
[29] H. Sadighi Dizaji, S. Jafarmadar, M. Abbasalizadeh, S. Khorasani, Experiments on air bubbles injection into a vertical shell and coiled tube heat exchanger; exergy and NTU analysis, Energy Convers. Manag. 103 (Oct. 2015) 973–980, https://doi.org/10.1016/j.enconman.2015.07.044.
[30] A. Moosavi, M. Abbasalizadeh, H. Sadighi Dizaji, Optimization of heat transfer and pressure drop characteristics via air bubble injection inside a shell and coiled tube heat exchanger, Exp. Therm. Fluid Sci. 78 (Nov. 2016) 1–9, https://doi.org/10.1016/j.expthermflusci.2016.05.011.
[31] E. Eder, M. Preißinger, Experimental analysis of the humidification of air in bubble columns for thermal water treatment systems, Exp. Therm. Fluid Sci. 115 (Jul. 2020) 110063, https://doi.org/10.1016/j.expthermflusci.2020.110063.
[32] H.M. Abd-ur-Rehman, F.A. Al-Sulaiman, A novel design of a multistage stepped bubble column humidifier for the humidification of air, Appl. Therm. Eng. 120 (Jun. 2017) 530–536, https://doi.org/10.1016/j.applthermaleng.2017.04.021.
[33] H. Inaba, S. Aoyama, N. Haruki, A. Horibe, K. Nagayoshi, Heat and mass transfer characteristics of air bubbles and hot water by direct contact, Heat Mass Tran. 38 (6) (Jun. 2002) 6, https://doi.org/10.1007/s002310100200.
[34] M.A.S.M. Yunos, N.K.A. Halim, S.A. Hussain, H.M. Yussof, S. Sipaun, Investigations of bubble size, gas hold-up, and bubble rise velocity in quadrilateral bubble column using high-speed camera, Am. J. Eng. Technol. Soc. 4 (1) (2017) 5–15.
[35] G. Besagni, F. Inzoli, Comprehensive experimental investigation of counter-current bubble column hydrodynamics: holdup, flow regime transition, bubble size distributions and local flow properties, Chem. Eng. Sci. 146 (Jun. 2016) 259–290, https://doi.org/10.1016/j.ces.2016.02.043.
[36] D.D. McClure, C. Wang, J.M. Kavanagh, D.F. Fletcher, G.W. Barton, Experimental investigation into the impact of sparger design on bubble columns at high superficial velocities, Chem. Eng. Res. Des. 106 (Feb. 2016) 205–213, https://doi.org/10.1016/j.cherd.2015.12.027.
[37] M.R. Rampure, A.A. Kulkarni, V.V. Ranade, Hydrodynamics of bubble column reactors at high gas velocity: experiments and computational fluid dynamics (CFD) simulations, Ind. Eng. Chem. Res. 46 (25) (Dec. 2007) 25, https://doi.org/10.1021/ie070079h.
[38] H. Miyashita, S. Yamaguchi, K. Kita, Experimental Investigation on Bubble Cooling for Large Amount of Heated Waste Water, Bulletin of Faculty of Engineering Toyama University, Takaoka, Japan, 1982.
[39] C. Boßer, D. Sedarsky, Verified PEMFC heavy-duty long-haul truck vehicle model with thermal management limitations of conventional cooling systems, Appl. Therm. Eng. 280 (Dec. 2025) 128025, https://doi.org/10.1016/j.applthermaleng.2025.128025.
[40] F.P. Incropera, D.P. DeWitt, T.L. Bergman, A.S. Lavine (Eds.), Fundamentals of Heat and Mass Transfer, 6, Wiley, Hoboken, NJ, 2007.
[41] e.V. VDI (Ed.), VDI Heat Atlas, second ed., Springer Berlin Heidelberg, 2010 https://doi.org/10.1007/978-3-540-77877-6.
[42] SV7050, Ifm electronic gmbh, datasheet [Online]. Available: https://www.ifm.com/de/en/product/SV7050. (Accessed 4 April 2025).
[43] NI-9203, National instruments corp., datasheet [Online]. Available: https://www.ni.com/sv-se/shop/model/ni-9203.html. (Accessed 4 April 2025).
[44] T.W. Lee, Thermal and Flow Measurements, CRC Press, 2008.
[45] FCO510 Micromanometer, Furness controls limited, datasheet [Online]. Available: https://www.bissistem.com/furness/files/fco510-laboratuvar-tipi-akis-olcer.pdf. (Accessed 9 October 2025).
[46] C.L. Hollingshead, M.C. Johnson, S.L. Barfuss, R.E. Spall, Discharge coefficient performance of venturi, standard concentric orifice plate, V-cone and wedge flow meters at low reynolds numbers, J. Pet. Sci. Eng. 78 (3) (Sep. 2011) 559–566, https://doi.org/10.1016/j.petrol.2011.08.008.
[47] Svenska institutet för standarder, European Commitee for Standardization, *Measurement of Fluid Flow by Means of Pressure Differential Devices Inserted in Circular cross-section Conduits Running Full*, SS-EN ISO 5167-1-4:2022, Jun. 2022.
[48] s.r.o. Aptec production, Alfa Laval Copper Brazed Plate Heat Exchanger, CB110-90H-F, Technical Specifications, Mar. 2024 [Online]. Available: https://aptec.international/wp-content/uploads/2024/03/EN-625-kW-8050-1060-CB110-90H.pdf. (Accessed 16 September 2025).
[49] F. Barbir, PEM Fuel Cells: Theory and Practice, second ed., Elsevier/Academic Press, Amsterdam ; Boston, 2013.
[50] WP150 HV, EMP, datasheet [Online]. Available: https://www.emp-corp.com/product/wp150-high-voltage/. (Accessed 12 November 2024).
[51] C. Doppler, B. Lindner-Rabl, Fuel cell trucks: thermal challenges in heat exchanger layout, Energies 16 (10) (Jan. 2023) 10, https://doi.org/10.3390/en16104024.
[52] M. Wagenblast, et al., Design and analysis of a spray cooling system for a heavy-duty fuel cell truck, SAE Tech. Pap. (Jun. 2022), https://doi.org/10.4271/2022-01-5054, 2022-01–5054.